김용준 석사 학위논문

Suppressed phonon conduction due to geometrically-induced evolution of transport characteristics from Brownian motion into Lévy walk

---

2021 년 1월

서울대학교 대학원

화학부

김용준

Suppressed phonon conduction due to geometrically-induced evolution of transport characteristics from Brownian motion into Lévy walk

---

지도교수 임종우

이 논문을 김용준 석사 학위논문으로 제출함

2021 년 1월

서울대학교 대학원

화학부

김용준

김용준의 석사 학위논문을 인준함

2021 년 1월

위 원 장 김지환 (인)

부 위 원 장 임종우 (인)

위 원 장혜진 (인)

Abstract

Suppressed phonon conduction due to geometrically-induced evolution of transport characteristics from Brownian motion into Lévy walk

Yongjoon Kim
Department of Chemistry
The Graduate School
Seoul National University

According to Moore's Law, the number of transistors per unit area has been doubled for every two years making the distance between source and drain become nearly 7 nm. As the dimensions are reduced to few nanometers, thermal conduction is suppressed compared to that of bulk, making thermal management complicated. High performance of CPU now relies on fine heat dissipation, thermal conductivity. The key to improve lifetime and performance depends on the fundamental understand of phonon conduction in silicon nanostructure.

Reduction of thermal conductivity, called size effect, is well understood in volumetrically homogeneous structures such as thin film and nanowire, with Boltzmann transport model and boundary scattering. On the other hand, inhomogeneous structures having uneven cross section along net heat flux direction, reduction mechanism is much more complicated showing discrepancy between experimental work and model prediction calling question to fundamental suppression mechanism.

Here, we use inhomogeneous nanoladders that consist of two straight beams orthogonally connected with bridges to systematically investigate phonon conduction. Measurement are conducted with suspended

membrane, electrothermal method for the thermal characterization of nanoribbon, nanowire, nanobeam structures. Modeling of thermal transport is performed with Callaway-Holland model and diffusive phonon scattering in computational space. As the ratio of the cross-sectional area for the line-of-sight channel along straight beams to that for bridges is modulated from ~5.3 to ~1, we find an unusual crossover in thermal conductivity characteristics. Together with self-consistent statistical analysis of phonon free paths, we find that the phonon transport in our nanoladders along the line-of-sight channel is dictated by Lévy-walk conduction as a result of scattered phonons getting filtered into bridges where Brownian motion of phonon dominates.

Our work shows that phonons can be selectively filtered by carefully engineering the volumetric ratio of heterogeneous structures in non-line-of-sight directions and minimizing phonon transport length within a given axial angle, enabling a powerful method to manage nanoscale heat in a non-diffusive manner.

---

keywords : Nanoladder, Thermal conductivity, Phonon, Lévy walk, Mean free path, Shape parameter, Free path distribution

Student Number **: 2019-26383**

Table of contents

1. Introduction

Understanding nanoscale phonon conduction mechanism is essential in a wide range of semiconductor applications, such as nanoelectronics[1, 2], optoelectronics[3, 4], and energy conversion devices[5, 6]. In the context of phonon conduction, nanostructures can be broadly categorized based on the uniformity of the cross-sectional area along the predominant direction of heat flow. A typical example of the structures with uniform cross-sectional area includes thin films,[7-10] nanobeams,[11] and smooth nanowires,[12-15] showing a significant reduction in thermal conductivity compared to that in the bulk counterpart. Such reduction in thermal conductivity is predominantly dictated by quasi-ballistic phonon transport in the line-of-sight (LOS) channel, which have substantially contributed to establishing a microscopic phonon conduction model.[16, 17] However, numerous nanostructures show anomalous heat conduction with increasing its complexity, calling questions in the suppression mechanisms on phonon transport.[18, 19]

It is generally accepted that the LOS channel is a primary heat conduction path, and its cross section dictates the thermal conductivity in a quasi-ballistic transport regime. With increased complexity of nanostructure, the thermal conductivity is observed to deviate from that of the LOS channel.[20, 21] A key feature associated with such enhanced suppression is that phonon flux is no longer one dimensional due to geometrical perturbations. The length scale of this perturbation ranges from angstrom to hundreds of nanometer, which is on the order of phonon mean free path (MFP). Various reduction mechanism has been suggested to explain the suppressed thermal conductivity in these complex nanostructures, with a focus on the interplay between phonon and the nanostructures. For example, previous reports on nanowires with few nanometer order disorder[22, 23] in the cross-sectional area as well as on phononic films[24-26] with periodic nanoscale holes suggest that the suppression can be associated with the wave-like effects of phonons, atomic defects, and backscattering.[27, 28] On the other hand, in fishbone structures, a nanobeam with orthogonally protruded pillars, or in corrugated nanowire with a series of periodically folded structure along the sidewall, the reduction of thermal conductivity is attributed to Sharvin resistance at the ballistic regime[29] and Lévy walk

transport characteristic.[30] In addition, it has been further shown that in bare nanoladder structures,[31] a nanobeam with nanobridges and a single row of pores, bridges constitute a thermally dead volume.[32] The above-mentioned reduction mechanisms are still under debate, calling for further studies on the origin of phonon reduction mechanism in complex nanostructures beyond the conventional phonon transport picture following Brownian motion.

Here, we investigate the evolution of thermal transport characteristics along the line-of-sight channel in nanoladders with a periodically varying cross-sectional area. Specifically, we prepare two sets of samples: 1) a set of nanobeams with varying cross-sectional area and 2) a set of two identical nanobeams connected with a series of orthogonally-placed bridges, resembling a ladder. With respect to the predominant heat direction, thermal transport in nanoladders consists of two regimes, line-of-sight (LOS) and bridges, which are connected orthogonally, while the nanobeams only have one LOS channel. Nanoladder is considered a series of repeating unit cells as illustrated in **Figure 1**a. Phonons contributing to the net transfer across the unit cell can be categorized into two groups: those traveling directly across the unit cell, and those fully thermalized within bridges. To quantify the relative contribution of each component to the thermal conduction, we deliberately design our samples by modulating the cross-section ratio of the LOS channel to bridges, ranging from ~1 to 5.29. Using a combination of Boltzmann transport equation with Monte Carlo approach, we model the phonon transport in our samples and find that the mean free path is determined by the volume ratio of the inhomogeneous structures. We further analyze a statistical distribution of phonon free paths to investigate its transport characteristics as well as its impact on resultant mean value.

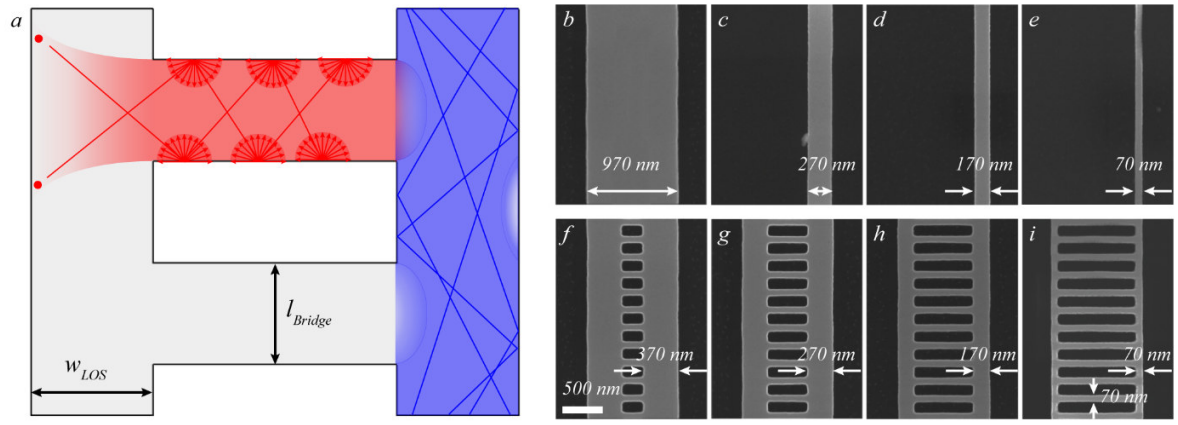

Figure 1. (a) An illustration of two characteristic phonon paths in nanoladders: the predominant phonon transport along the line-of-sight (LOS) channels (shaded blue region) and phonons captured within the bridge (shaded red region). (b-e) Scanning electron microscopy (SEM) images of straight beams with w = (b) 970 nm, (c) 270 nm, (d) 170 nm, and (e) 70 nm. (f-i) SEM images of nanoladders with w_{LOS} = (f) 370 nm, (g) 270 nm, (h) 170 nm, and (i) 70 nm.

2. Experimental

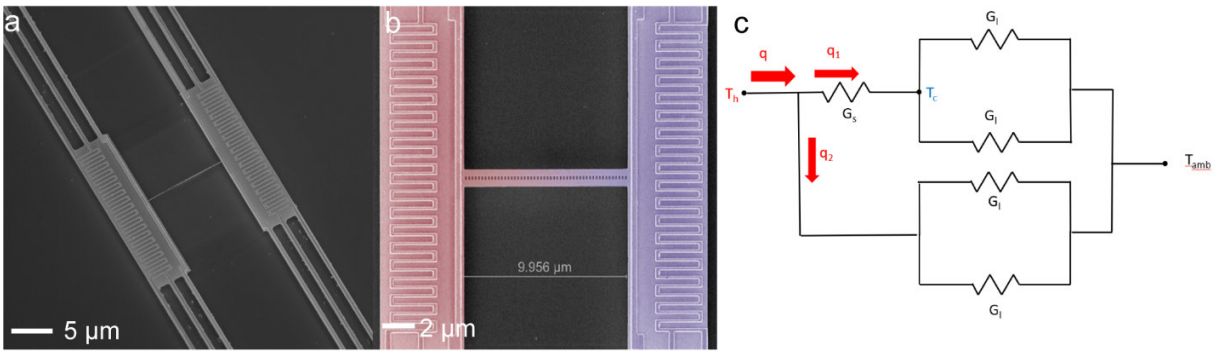

Figure 2. (a) SEM overview image of suspended membranes for electrothermal measurement. (b) Colored image of membranes, red color for heated membrane, blue color for sensing membrane. (c) Thermal circuit of electrothermal measurement system.

Electrothermal measurement: For the measurement of thermal conductivity, electrothermal measurement is conducted with suspended membrane. As shown in **Figure 2**a, two membranes are suspended with six legs, serpentine Pt wire deposited onto them. When current flows through Pt coil of one side, Joule heat is generated. Nanostructure such as nanobeam, nanoribbon, nanomesh is located between membranes so that heat can flow from heated membrane to non-heated membrane. As system approaches to steady state, heat conducted from hot platform represented as red color in Figure 2b to cold platform shown as blue color obeys governing equation of

$$q = \frac{kA(T_h - T_c)}{l} \quad (1a)$$

where q is heat transfer rate, k is thermal conductivity, A is cross section of nanowire, T_h is temperature of hot side, T_c is temperature of cold side and l is the length of nanowire. Generated Joule heat satisfies equation of

$$q = I\frac{V_{coil} + V_{coil+leg}}{2} \quad (1b)$$

where I is current, V_{coil} is the voltage of the coil, the serpentine part and $V_{coil+leg}$ is voltage of serpentine part and legs. Pt coil serves as thermometer because electrical resistance and the temperature of it satisfies equation of

$$R = R_0(1 + \alpha\Delta T) \quad (2)$$

where R is electrical resistance, R_0 is electrical resistance when there is no current, α is temperature coefficient of resistance(TCR) and is material property and ΔT is temperature change.

Thermal conductance ($G = \frac{kA}{l}$) then can be calculated by dividing the Joule heat by temperature change of each islands from the electrical resistance.

In real system, generated Joule heat in coil not only flows through the nanowire but flows through the legs. As a result, thermal circuit of the system is more complex and represented in Figure 2c. Generated Joule

heat can be divided into two: 1) heat passes nanostructure and then passes leg (q_1) and 2) heat pass only leg (q_2). According to the Fourier's law, in the former case,

$q_1 = \frac{G_l G_s}{G_l+G_s}(T_h - T_c)$ and the latter $q_2 = G_l(T_h - T_c)$. By representing equation with T_h, T_c, ambient temperature(T_{amb}) and q, equation becomes

$$T_h - T_{amb} = \frac{2G_l+G_s}{4G_l(G_l+G_s)}q \tag{3a}$$

and

$$T_c - T_{amb} = \frac{G_s}{4G_l(G_l+G_s)}q \tag{3b}$$

by letting the slope of T_h vs q plot and T_c vs q plot as m_1 and m_2, thermal conductance G_s is given as

$$G_s = \frac{m_2}{(m_1-m_2)m_1} \tag{4}$$

To prevent heat transfer through convection, chamber is maintained with vacuum condition. Radiation heat transfer is negligible compared to conduction, when the temperature different between each island is lower than 10 K.

Device Fabrication : We fabricate silicon nanostructures on a silicon-on-insulator (SOI) wafers (Soitec Inc.) comprised of silicon layer and buried oxide layer (BOX) having thickness of 340 nm and 1 μm respectively. First, the silicon layer is thinned down to ~78 nm, using thermal oxidation and consecutive removal of oxide by wet etching process (6:1 buffered oxide etchant is used). ~25 nm thick Al_2O_3 is deposited on the top of the silicon layer for electrical insulation between metal line and the silicon below. For sample area, a window of 10 μm ×20 μm is patterned between membranes by photolithography, and a wet etching processes is used to remove the insulation layer. Nanostructures are patterned in this open area using electron beam lithography, and a reactive ion etching(RIE) is used to remove the silicon in the non-sample area. Pt heater/thermometer lines and contact pads are patterned onto each platform for electrical access by using a combination of electron beam lithography and photo lithography. A lift-off process is followed after deposition of Cr and Pt of ~5 and ~40 nm thickness using electron beam metal

evaporation. The BOX layer in the surrounding area of the membranes and legs are etched using RIE, and they are suspended by using gaseous hydrogen fluoride (HF) etching. All dimensions are measured using scanning electron microscopy (SEM) after fabrication and for the measurement of silicon nanostructures.

Simulation Process: To do statistical analysis and plot trajectory, we record the position and velocity of phonon at scattering events. To confirm the distribution of free path, we obtain histogram with respect to free path, with MATLAB, having bin number of 500 at the interval of (0, 970) nm. By normalizing the histogram with total phonon number, probability mass function of the simulation is given as

$$y\left(\frac{X_i+X_{i+1}}{2}\right) = h_i \ (i = 1,2,3 \dots, n-1) \qquad (5)$$

where n is the number of the bin, X_i is free path of each interval of histogram, h_i is probability. By using least square fitting method, probability density function of Pareto distribution $f(X) = \frac{\alpha L_C^{\alpha}}{X^{\alpha+1}}$ is fitted to the **Equation** (5), providing shape parameter. To represent the trajectory of phonon flights, we use patch function in MATLAB, which regards line as polygon so that we can put transparency to the line. we set the end of the trajectory as "NaN" so that trajectory shows unclosed polygon with transparency of 20%.

3. Result and Discussion

As shown in Figure 1 (b-i), we carefully prepare the following two sets of samples: 1) straight beams and 2) nanoladders (consisting of two straight beams placed in parallel and connected orthogonally using bridges). For straight beams, we vary the aspect ratio of the cross section from ~0.9 to ~13.9 by modulating the width w_{LOS} from ~70 nm to ~970 nm, while keeping the thickness t at ~78 nm. Similarly, for nanoladders, we vary the width of two straight beams from ~70 nm to ~370 nm, and ~70 nm by ~78 nm sized bridges are placed between these beams with a periodicity of 200 nm. Here, the bridge width l_{bridge} is ~70 nm.

Accordingly, the volume ratio of the LOS channels to bridges ranges from ~0.48 to ~9.2 in our nanoladders, and both sets of samples have identical LOS channels. Note that we ensure that both sets of samples are 10 μm long such that phonon transport is diffusive along the LOS channels.

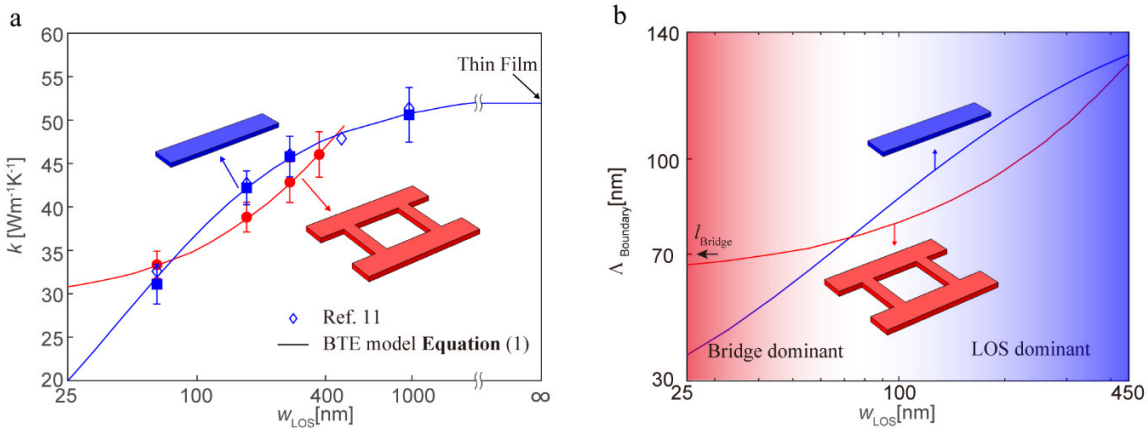

Figure 3. (a) Thermal conductivity of nanoladders (solid red circles) and straight beams (solid blue squares) as a function of the line-of-sight channel width w_{LOS}. The solid lines are the model prediction based on Boltzmann transport equation. (b) Mean free paths for boundary scattering in nanoladders (red solid line) and straight beams (blue solid line) versus w_{LOS}.

Figure 3a shows that as the cross-sectional area of the LOS channel is decreased, thermal conductivity decreases from ~50 to ~30 W m^{-1} K^{-1} and from ~45 to ~33 W m^{-1} K^{-1}, for straight beams and nanoladders, respectively. Note that for straight beams, we find that as the aspect ratio is increased, the thermal conductivity approaches the thin-film limit, verifying the validity of our measurements.[33] The monotonic decrease in both sets of samples indicates that the cross-sectional area of the LOS channel is the predominant factor that dictates the overall thermal conductivity in our samples, as discussed in previous studies.[34-36] However, we find a crossover of the thermal conductivity between the two sets despite the

identical cross-section of LOS channel. Thermal conductivity in the nanoladders is smaller than that of straight beams when $w_{LOS} > l_{bridge}$, whereas the relative magnitude is reversed when $w_{LOS} < l_{bridge}$.

To better understand the phonon conduction in between straight beams and nanoladders, we model the thermal conductivity based on Boltzmann transport equation as[37, 38]

$$k = \frac{1}{6\pi^2}\sum_i \int C_{V,i}(q) v_i(q)^2 \tau_i(q) dq \quad (6)$$

where i is the mode of phonon, q is the phonon wavevector, C_V is the volumetric heat capacity, v is the group velocity, and τ is the relaxation time. Born-van Karman sine type dispersion relation is used. Phonon mean free path Λ is defined as $\Lambda = v \times \tau$, and can be derived using Matthiessen's rule as $\tau = (\tau_U^{-1} + \tau_I^{-1} + \tau_B^{-1})^{-1}$, where $\tau_U$is the Umklapp scattering rate defined as $\tau_U^{-1} = Aw^2 Texp(-\frac{B}{T})$, and τ_I is the impurity scattering rate defined as $\tau_I^{-1} = Dw^4$. The boundary scattering rate $\tau_B$is estimated by simulating phonon particles using Monte-Carlo schemes. To determine the parameters A, B and D, we fit **Equation** (6) to the experimental data of straight beams. For the best fit, A, B and D is given as 1.81×10^{-19} sK^{-1}, 151 K and 8.34×10^{-45} s^3, respectively (see Supporting Information for detailed Boltzmann transport model). We apply the fitted value to predict thermal conductivity of nanoladders, and the fit shows agreement with our experimental data within ~2%. This agreement indicates that the model captures the characteristics of phonon transport in our samples as seen in Figure 3a. More importantly, the model prediction clearly shows the crossover of the thermal conductivity between nanoladders and straight beams.

We further investigate the dependence of phonon mean free path on boundary scattering, which dictates the thermal conductivity at given length scale of our samples. We plot the boundary scattering mean free path $\Lambda_{Boundary}$ in Figure 3b, which shows a clear crossover behavior between the nanoladders and straight beams, similar to the observed thermal conductivity. On the one hand, when $w_{LOS} > l_{Bridge}$, $\Lambda_{Boundary}$ in nanoladders is smaller than in straight beams as shorter MFPs are introduced from the bridges. On the other hand, when $w_{LOS} < l_{Bridge}$, $\Lambda_{Boundary}$ in the nanoladders asymptotically saturates at a constant value as w_{LOS}

is decreased, while it decreases monotonically in the straight beam counterpart. The asymptotic limit of the nanoladders is mainly dictated by the geometrical dimension of the bridge, which introduces a constant scattering cross-section. This indicates that $\Lambda_{Boundary}$ in nanoladders is nearly determined by the volumetric contribution of heterogeneous structures regardless of their relative contribution to the net heat flux. As such, the critical dimensions of the bridges serve as a source of free paths while the contribution to net heat flux from bridges is negligible.

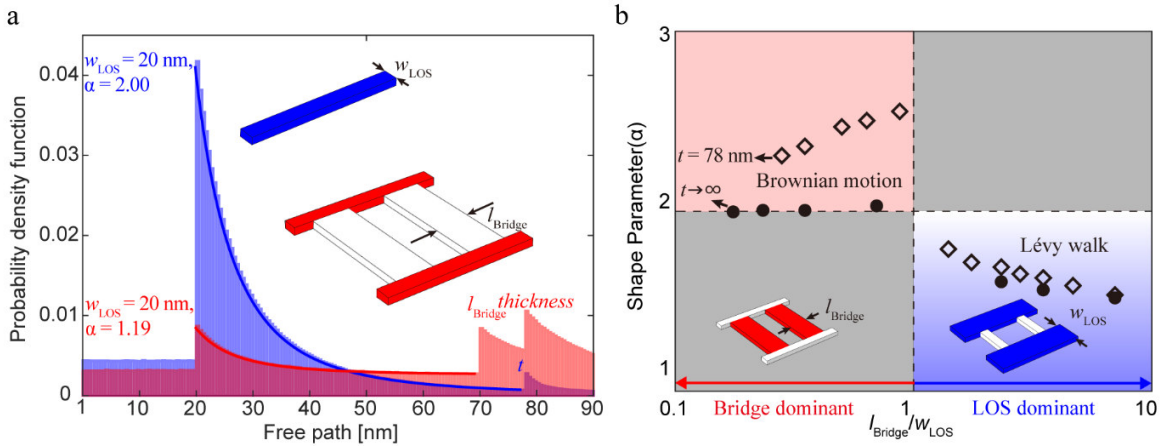

Figure 4. (a) Probability density function (PDF) of phonon free path in nanoladders. The red and blue colors correspond to the phonon free path in bridge and in LOS channel, respectively (w_{LOS} = 20 nm, thickness t = 78 nm, and bridge length l_{Bridge} = 70 nm). Note that the PDF peaks whenever free path coincides with the dimension of the characteristic features present in nanoladders. Each peak can be described in term of the characteristic length L_C and shape parameter α, which determines the decay profile of free paths. (b) α versus the ratio of l_{Bridge} to w_{LOS} in nanoladders. The dark solid grey color indicates the infinitely thick limit where thickness-dependent diffuse boundary scattering becomes negligible. For $\alpha > 2$, phonon transport is diffusive (red shaded region), but as α crosses 2, phonons display Lévy walk transport characteristics (blue shaded region).

We next statistically analyze the boundary scattering free path distribution in both nanoladders and straight beams. As can seen in **Figure 4**a, the free path distribution is expressed in terms of the probability

density function (PDF), which shows peaks at characteristic dimensions of the nanoladder and the straight beam – w_{LOS} and thickness t. Note that we choose w_{LOS} = 20 nm to emphasize the role of the LOS channel in free path distributions. We observe that the PDF of free paths for nanoladders is dramatically suppressed near 20 nm compared to that in the straight beams. In contrast, it is enhanced at ~70 nm (=l_{Bridge}) compared to that in the straight beams. Such conversion of weights in the PDF is mainly due to the phonons being trapped in the bridges, which occurs mostly for phonons traveling at a relatively large axial angle with respect to the predominant direction of heat flow along the LOS channel.[30]

To further obtain quantitative information on the transport characteristics, we interpret the PDF using Pareto distribution expressed as[39]

$$f(X) = \frac{\alpha L_C^{\alpha}}{X^{\alpha+1}}, \quad (7)$$

where $L_C = min(w_{LOS}, l_{bridge}, t)$ is the length scale of the smallest characteristic dimension present in the nanostructure, X is the free path, and α is the shape parameter which reflects the phonon transport mechanism: ballistic transport for α = 1, Lévy walk for $1 < \alpha < 2$, and Brownian motion for $\alpha = 2$. We note that Pareto distribution has been studied in Bose-Einstein processes, such as thermal transport in SiGe, InGaAs alloys[40-42] as well as in silicon nanowires at low temperatures.[30] Using the Pareto distribution framework, we fit the simulated PDFs of free paths in nanoladders and extract the shape parameter α as a function of the ratio of the predominant critical dimensions, w_{LOS} to l_{Bridge}. We find that for $w_{LOS} > l_{Bridge}$, α is larger than 2 and α also becomes smaller than 2 when $w_{LOS} < l_{Bridge}$ as seen in Figure 4b. Note that this analysis focuses on the PDF near the smallest characteristic dimension present in the nanostructure to avoid the interplay with other larger characteristic dimensions. We can therefore deduce that the bridge region is dominated by Brownian motion ($\alpha > 2$), while the LOS channel displays Lévy walk characteristics ($\alpha < 2$). We note that heat conduction typically follows Brownian motion. For example, in the case for infinitely thick samples, the bridge region shows perfect Brownian motion, as indicated by α = 2. Furthermore, we

find that straight beams also show Brownian motion ($\alpha = 2$) as opposed to the LOS channels in nanoladders. These observations suggest that the characteristics of phonon transport is converted from Brownian motion to Lévy flight along the LOS channel in our nanoladders by bridging the parallel channels.

We estimate the contribution of Lévy walk character on the phonon mean free path $E(X)$ using Pareto distribution as

$$E(X) = \int_{L_c}^{\infty} X \frac{\alpha L_c^{\alpha}}{X^{\alpha+1}} dX = \frac{\alpha}{\alpha-1} L_c \ (\alpha > 1), \tag{8}$$

where X is the free path, α is the shape parameter, and L_c is the characteristic length for the boundary scattering. We note that $\alpha = 2$ corresponds to the Brownian motion regime, while $1 < \alpha < 2$ for Lévy walk. As can be seen in **Figure 5**, the degree of boundary scattering contribution to the mean free path depends on the phonon transport characteristics, i.e. α. This suggests that phonons displaying Lévy walk characteristics are likely to have a longer mean free path than that for Brownian motion.

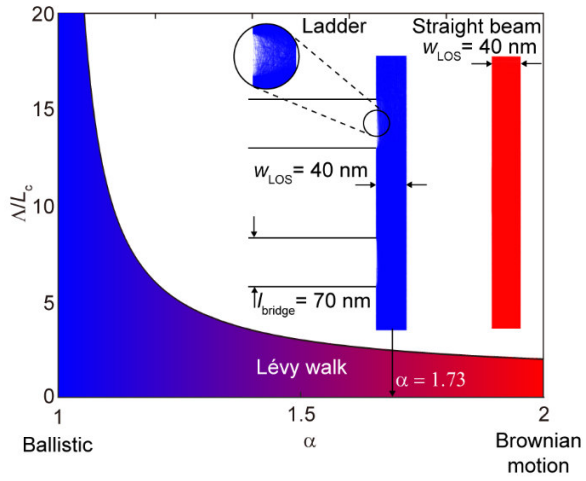

Figure 5. Mean free path normalized to the critical dimension L_C as a function of the shape parameter α. The region shaded in red color indicates the Lévy walk regime ($\alpha < 2$) while Brownian motion is found at $\alpha = 2$. The inset shows simulated phonon trajectory in both Lévy walk (left) and Brownian motion (right) regimes. We note that the inset for Lévy walk corresponds to $\alpha = 1.73$.

We further visualize phonon paths along the LOS channels in both nanoladders and straight beams by simulating 3×10^4 phonons in a 3D computational space, which are projected on a two-dimensional plane as seen in the inset of Figure 5. It is noteworthy that the collective set of phonon trajectories renders dead space at the entrance of the bridges. As such, phonons propagating along the LOS channel is likely to form an artificially corrugated structure, with those propagating with narrow axial angle following Lévy walk characteristics. Given the statistical analysis above, we suggest that phonons propagating with broad axial angles get dominantly trapped within bridges in our nanoladder and are dictated by the boundary scattering therein. As w_{LOS} is decreased, more portion of phonons with large-angle scattering are likely to be trapped in the bridges. The remaining phonons with narrow axial angles contribute to the decrease in the shape parameter as well as the increase in the mean free path in the LOS channel. However, the overall thermal conductivity of the nanoladder is suppressed as the majority of phonons are trapped in Brownian motion dominated bridges; this suppression becomes further pronounced as the critical dimension of bridges is comparable to or smaller than that of the LOS channel.

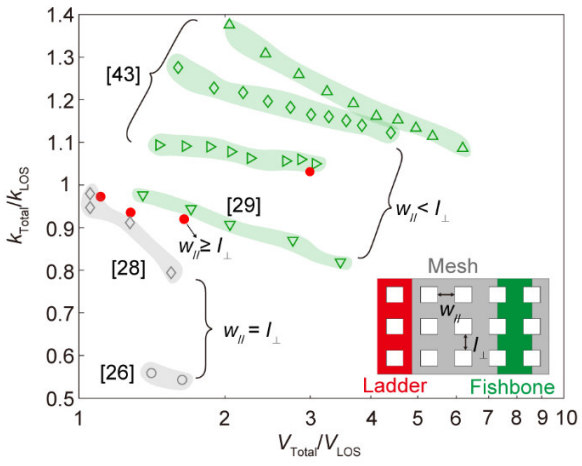

Figure 6. A collective experimental data for thermal conductivity in various nanostructures with non-uniform cross section along the primary heat flux direction. Thermal conductivity in each nanostructure is normalized to that in the corresponding line-of-sight channel. Data points located in green shaded area are the values having $w_{//} < l_{\perp}$, in gray area are the values having $w_{//} = l_{\perp}$. Solid red dots, data point of this work satisfies $w_{//} \geq l_{\perp}$, gray diamond are data points with various periodicity.

Finally, we extend our discussion on the impact of geometrical heterogeneity on phonon transport in the context of previous studies on other nanostructures, such as nanomeshes[26, 28] and fishbone nanowires[29, 43] as shown in inset of **Figure 6**. These structures can be decomposed into the LOS channel and the other which orthogonally aligned with respect to the LOS, and the corresponding critical dimensions are set to be $w_{//}$ and $l_{\perp}$, respectively. Figure 6 shows the thermal conductivity of the above-mentioned nanostructures normalized to that for the LOS channel as a function of the volumetric ratio of the nanostructure to that for the LOS channel. For the nanomeshes, the critical dimensions are the same $l_{\perp} = w_{//}$, and the thermal conductivity decreases with increasing volumetric density of non-LOS channel. For the fishbones with $l_{\perp} > w_{//}$, the thermal conductivity decreases with increasing the volume ratio, V_{Total} to V_{LOS}, despite increasing volumetric contribution of non-LOS channel. In both cases, as the critical dimension with non-LOS channel is larger than that along the LOS channel, the volumetric change fails to capture the suppression with increasing volume ratio of the non-LOS channel. Given structures, the phonon conduction through LOS channel is also likely to show Lévy-walk characteristics, increasing the mean free paths along the channel. Above mentioned factors fail to explain the reduction. As such, the further suppression with increasing volume of non-LOS channel is due to the increasingly trapped phonons with the non-LOS channel, forced to follow Brownian motion within the regime.

4. Conclusion

In summary, we investigate phonon transport mechanism in silicon nanoladders and nanobeams. We observe a crossover in the thermal conductivity between the nanoladders and straight beams as a function of the volumetric ratio of the bridge to LOS channels. A model prediction based on Boltzmann transport suggests that non-LOS channel contributes as a major source of phonon boundary scattering despite its negligible contribution to the net heat flux. Furthermore, a statistical analysis on the distribution of free paths suggests that the bridges convert the transport characteristics of the LOS channel. We quantitatively identify this conversion using Pareto –distribution framework as phonons traversing along the LOS channel following Lévy walk process, while those trapped in bridges showing a diffusive behavior. As a result, phonons in the LOS channel of the nanoladders have a relatively long mean free path as bridges capture large-angle phonons with respect to the axial direction. Finally, we extend our observation to the other nanostructures with orthogonal geometric obstructions, such as nanomesh and fishbone nanowire. This work unravels a long-lasting question for the interplay between phonons and nanostructures, contributing to a comprehensive model for complex nanostructures.

5. Supporting information

1. Phonon dispersion for the model based on Boltzmann transport equation

For the thermal conductivity model based on Boltzmann transport equation(BTE), we use Born-von Karman-Slack(BvKS) phonon dispersion relation model.[44] In BvKS model, angular frequency ω is

$$\omega = \omega_{max} \sin\left(\frac{\pi q}{2q_{max}}\right) \quad (9)$$

where q is wave vector, ω_{max} is maximum frequency in each phonon mode, and q_{max} is cutoff wavevector corresponding to ω_{max}. The group velocity v_g is given as the partial derivative of **Equation** (9) with respect to q

$$v_g = \frac{\pi\omega_{max}}{2q_{max}}\cos\left(\frac{\pi q}{2q_{max}}\right) \quad (10)$$

In BvkS model, three acoustic branches are approximated to one effective branch, having q_{max} and ω_{max} of 1.14×10^{10} m^{-1} and 4.415×10^{13} s^{-1} respectively. We neglect the contribution of optical phonons to thermal conductivity.[45]

2. Ray-tracing model to predict mean free path due to boundary scattering

The mean free path due to boundary scattering is calculated by simulating 10^4 phonons in a three-dimensional computational space. We define a unit cell of both ladders and beams as seen in **Figure 7**. The positions of phonons are uniformly generated at a plane y = 0, represented as orange hatched area of Figure 7, and those direction vectors are set to be

$$v_x = sin\theta cos\Phi \quad (11a)$$

$$v_y = cos\theta \quad (11b)$$

$$v_z = sin\theta sin\Phi \quad (11c)$$

where θ and Φ are polar angle and azimuthal angle respectively to a plane-normal vector (0,1,0). Given positions and directions, we calculate the next position by determining the minimum distance of the particles with given boundaries. At the position with the minimum traveling distances, the directions of the phonons are scattered diffusely by setting its direction following Lambertian cosine Law as illustrated in **Figure 8**. In Figure 8, an incident phonon is shown as black arrow, and the red arrows indicate the distribution of reflected phonons. Mathematically, both azimuthal angle Φ and polar angle θ for scattered phonons are given to be

$$sin\theta = (\text{rand})^{1/2} \quad (12a)$$

$$cos\theta = (1\text{-}\ sin^2\theta)^{1/2} \quad (12b)$$

$$\Phi = 2\pi \times \text{rand} \quad (12c)$$

where rand is random number between 0 and 1. We repeat the simulation until the total number of scattering events reaches 10^4 to capture the transport characteristics.

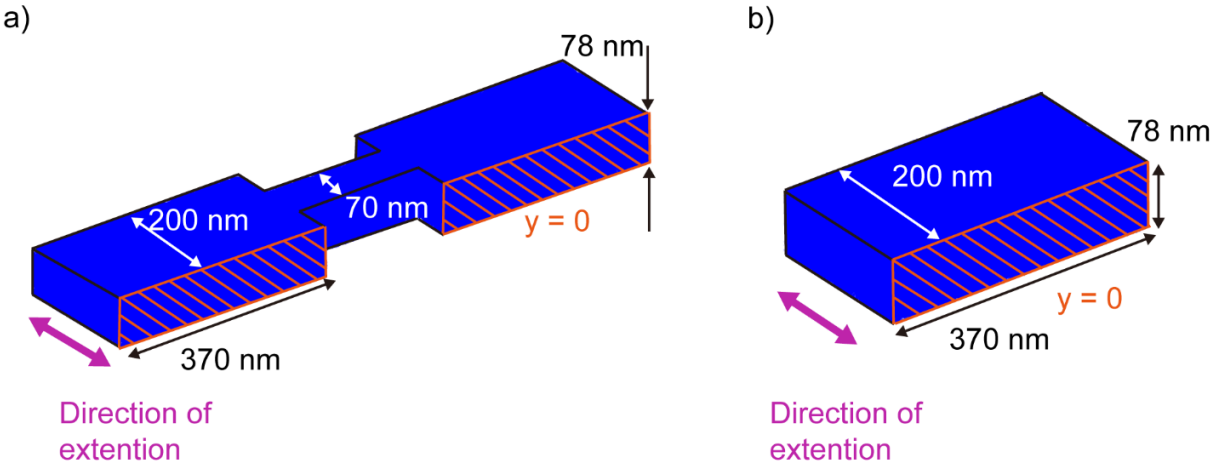

Figure 7. Position of phonons within unit cell boundaries of a) a ladder and b) a beam in three-dimensional space. Phonons follow given scattering algorithm of ladder and beam having w_{LOS} = 370 nm. For computational convenience, phonons are represented in the unit cell of the nanostructures.

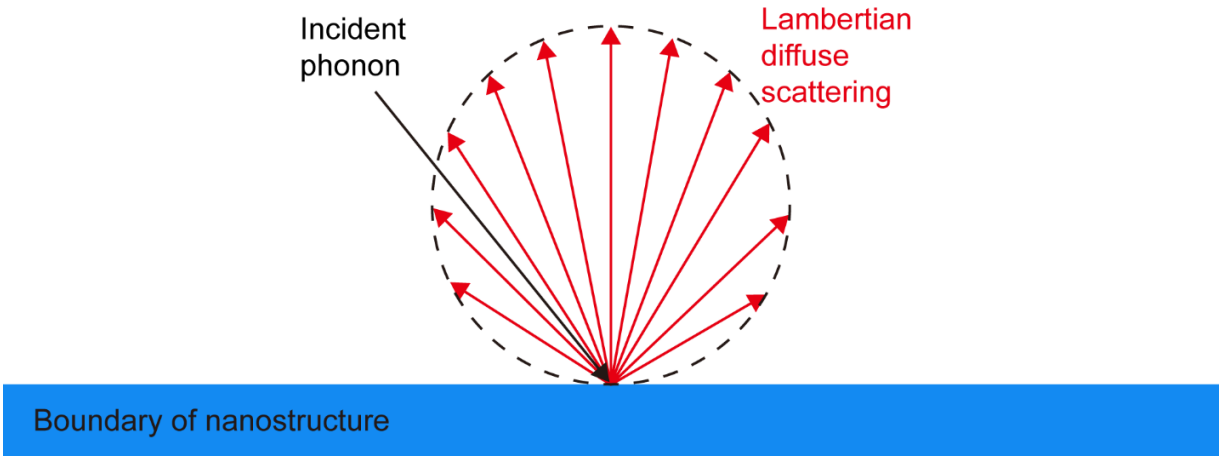

Figure 8. Schematic illustration of Lambertian diffuse scattering. Phonon represented as black arrow scatters at the boundary of the structure, colored blue. Traveling direction after scattering event follows Lambertian distribution, represented as red arrows.

3. Uncertainty Analysis

We quantify the uncertainty of our measurements using

$$\left(\frac{\Delta k}{k}\right)_{Total} = \sqrt{\left(\left(\frac{\Delta k}{k}\right)_{var,1}\right)^2 + \left(\left(\frac{\Delta k}{k}\right)_{var,2}\right)^2 \cdots} \quad (13)$$

where k is the thermal conductivity, and *var* indicates each component contributing to the uncertainty. The total error is predominantly dictated by the uncertainty of sample dimensions as the quantification of dimensions are limited by spatial resolution of scanning electron microscope (SEM) measurements. In **Table S1**, we summarize both the uncertainty and the dimension namely thickness, w_{LOS}, and l_{Bridge} as well as the propagation of those uncertainty to total error. We note that the total error is less than ~8% of the thermal conductivity in this work.

Samples		k ($Wm^{-1}K^{-1}$)	t (±5 nm) error(%)	w_{LOS} (±5 nm) error(%)	l_{Bridge} (±5 nm) error(%)	Total error(%)
Beam	w_{LOS} = 70	31.1	4.02	6.54	-	7.68
	w_{LOS} = 170	42.2	3.67	5.27	-	6.42
	w_{LOS} = 270	45.8	3.37	4.31	-	5.47
	w_{LOS} = 970	50.6	3.27	3.75	-	4.97
Ladder	w_{LOS} = 70	33.4	4.09	5.29	5.70	8.79
	w_{LOS} = 170	38.8	3.68	5.09	2.94	6.93
	w_{LOS} = 270	42.9	3.50	4.72	1.80	6.15
	w_{LOS} = 370	46.0	3.49	4.35	1.54	5.79

Table 1. Geometrical uncertainty of nanoladder and nanobeam

4. Constriction and spreading resistance within a suspended island.

To consider the thermal resistance due to constriction and spreading of heat within an island, we estimate the resistances using numerical simulation, COMSOL. We compare two cases 1) sample only and 2) samples with supporting islands. The thermal resistance of the samples can be simply calculated using

$$R_{th} = \frac{\Delta T}{q} \tag{14}$$

where ΔT is temperature difference of hot membrane to cold membrane and q is heat transfer rate. For the resistance across samples with supporting islands, we build the suspended membrane structures as seen in **Figure 9**. The area of the membrane is 1.8 μm × 16.8 μm, and a metal heater is placed on top of the membrane. The thicknesses of materials are given to be 78 nm for silicon, 21 nm for alumina, 5 nm for Cr, and 40 nm for Pt. We consider the Cr and Pt as a single material to be Pt as Cr is used for adhesion layer. The thermal conductivity for Si, Al_2O_3, and Pt are 52.0, 1.50, and 35 $Wm^{-1}K^{-1}$, respectively [33, 46, 47]. With temperature difference of 10 K at the end of each island, the heat flux across the sample is calculated. The total thermal resistance is calculated by dividing heat transfer rate to temperature difference. As total thermal resistance contains thermal resistance of two islands, that of sample and that of spreading/constriction, constriction/spreading resistance is

$$R_{const} = R_{total} - 2R_{island} - R_{sample} \tag{15}$$

Thermal resistance of the sample and spreading/constriction resistances are summarized in Table S2.

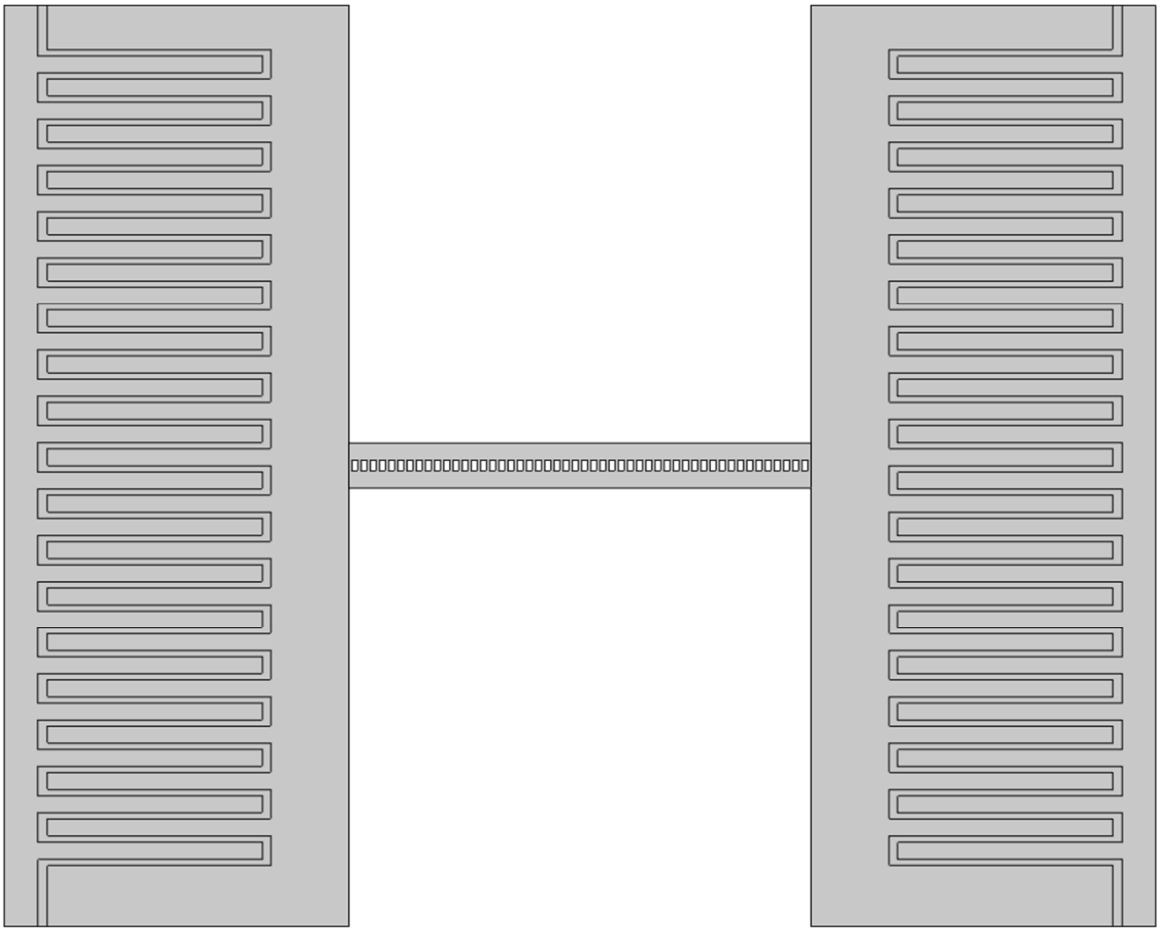

Figure 9. Structure of suspended membrane and nanoladder of w_{LOS} = 370 nm, used for spreading and constriction thermal resistance.

Structure		R_{const} ($\times 10^6$ KW^{-1})	R_{sample} ($\times 10^6$ KW^{-1})	R_{const}/R_{sample} (%)
Beam	w_{LOS} = 70	0.69	60.1	1.15
	w_{LOS} = 170	0.55	17.1	3.93
	w_{LOS} = 270	0.48	10.5	4.60
	w_{LOS} = 970	0.29	2.7	10.5

Ladder	w_{LOS} = 70	0.34	26.3	1.30
	w_{LOS} = 170	0.34	8.8	3.88
	w_{LOS} = 270	0.34	5.3	6.41
	w_{LOS} = 370	0.34	3.9	8.69

Table 2. Thermal resistance of constriction and spreading, thermal resistance of sample and their ratio with respect to w_{LOS} of the ladder and beam.

[1] A. L. Moore, L. Shi, *Materials today* **2014**, 17, 163.
[2] E. Pop, *Nano Research* **2010**, 3, 147.
[3] H. H. Cheng, D.-S. Huang, M.-T. Lin, *Microelectronics Reliability* **2012**, 52, 905.
[4] X. Luo, R. Hu, S. Liu, K. Wang, *Progress in Energy and Combustion Science* **2016**, 56, 1.
[5] M. Browne, B. Norton, S. McCormack, *Renewable and Sustainable Energy Reviews* **2015**, 47, 762.
[6] M. Zebarjadi, *Scientific reports* **2016**, 6, 20951.
[7] W. Liu, M. Asheghi, *Applied Physics Letters* **2004**, 84, 3819.
[8] W. Liu, M. Asheghi, presented at Heat Transfer Summer Conference **2005**.
[9] Y. Ju, K. Goodson, *Applied Physics Letters* **1999**, 74, 3005.
[10] J. A. Johnson, A. Maznev, J. Cuffe, J. K. Eliason, A. J. Minnich, T. Kehoe, C. M. S. Torres, G. Chen, K. A. Nelson, *Physical review letters* **2013**, 110, 025901.
[11] W. Park, D. D. Shin, S. J. Kim, J. S. Katz, J. Park, C. H. Ahn, T. Kodama, M. Asheghi, T. W. Kenny, K. E. Goodson, *Applied Physics Letters* **2017**, 110, 213102.
[12] N. Mingo, *Physical Review B* **2003**, 68, 113308.
[13] N. Mingo, L. Yang, D. Li, A. Majumdar, *Nano Letters* **2003**, 3, 1713.
[14] D. Li, Y. Wu, P. Kim, L. Shi, P. Yang, A. Majumdar, *Applied Physics Letters* **2003**, 83, 2934.
[15] R. Chen, A. I. Hochbaum, P. Murphy, J. Moore, P. Yang, A. Majumdar, *Physical review letters* **2008**, 101, 105501.
[16] F. Yang, C. Dames, *Physical Review B* **2013**, 87, 035437.
[17] Y. Hu, L. Zeng, A. J. Minnich, M. S. Dresselhaus, G. Chen, *Nature nanotechnology* **2015**, 10, 701.
[18] S. Liu, X. Xu, R. Xie, G. Zhang, B. Li, *The European Physical Journal B* **2012**, 85, 337.
[19] A. Dhar, K. Saito, B. Derrida, *Physical Review E* **2013**, 87, 010103.
[20] P. E. Hopkins, C. M. Reinke, M. F. Su, R. H. Olsson III, E. A. Shaner, Z. C. Leseman, J. R. Serrano, L. M. Phinney, I. El-Kady, *Nano letters* **2011**, 11, 107.
[21] E. Dechaumphai, R. Chen, *Journal of Applied Physics* **2012**, 111, 073508.
[22] J. Lim, K. Hippalgaonkar, S. C. Andrews, A. Majumdar, P. Yang, *Nano letters* **2012**, 12, 2475.
[23] J. Lee, W. Lee, J. Lim, Y. Yu, Q. Kong, J. J. Urban, P. Yang, *Nano letters* **2016**, 16, 4133.

[24] D. Song, G. Chen, *Applied physics letters* **2004**, 84, 687.
[25] J. Nakagawa, Y. Kage, T. Hori, J. Shiomi, M. Nomura, *Applied Physics Letters* **2015**, 107, 023104.
[26] J.-K. Yu, S. Mitrovic, D. Tham, J. Varghese, J. R. Heath, *Nature nanotechnology* **2010**, 5, 718.
[27] S. Alaie, D. F. Goettler, M. Su, Z. C. Leseman, C. M. Reinke, I. El-Kady, *Nature communications* **2015**, 6, 1.
[28] J. Lee, W. Lee, G. Wehmeyer, S. Dhuey, D. L. Olynick, S. Cabrini, C. Dames, J. J. Urban, P. Yang, *Nature communications* **2017**, 8, 1.
[29] L. Yang, Y. Zhao, Q. Zhang, J. Yang, D. Li, *Nanoscale* **2019**, 11, 8196.
[30] R. Anufriev, S. Gluchko, S. Volz, M. Nomura, *ACS nano* **2018**, 12, 11928.
[31] R. Yanagisawa, J. Maire, A. Ramiere, R. Anufriev, M. Nomura, *Applied Physics Letters* **2017**, 110, 133108.
[32] W. Park, J. Sohn, G. Romano, T. Kodama, A. Sood, J. S. Katz, B. S. Kim, H. So, E. C. Ahn, M. Asheghi, *Nanoscale* **2018**, 10, 11117.
[33] M. Asheghi, M. N. Touzelbaev, K. E. Goodson, Y. K. Leung, S. S. Wong, *J Heat Trans-T Asme* **1998**, 120, 30.
[34] J. Tang, H.-T. Wang, D. H. Lee, M. Fardy, Z. Huo, T. P. Russell, P. Yang, *Nano letters* **2010**, 10, 4279.
[35] R. Anufriev, J. Maire, M. Nomura, *Physical Review B* **2016**, 93, 045411.
[36] R. Anufriev, A. Ramiere, J. Maire, M. Nomura, *Nature communications* **2017**, 8, 1.
[37] J. Callaway, *Physical Review* **1959**, 113, 1046.
[38] M. Holland, *Physical review* **1963**, 132, 2461.
[39] L. Amoroso, *Econometrica: Journal of the Econometric Society* **1938**, 1.
[40] B. Vermeersch, J. Carrete, N. Mingo, A. Shakouri, *Physical Review B* **2015**, 91, 085202.
[41] B. Vermeersch, A. M. Mohammed, G. Pernot, Y. R. Koh, A. Shakouri, *Physical Review B* **2015**, 91, 085203.
[42] M. Upadhyaya, Z. Aksamija, *Physical Review B* **2016**, 94, 174303.
[43] J. Maire, R. Anufriev, T. Hori, J. Shiomi, S. Volz, M. Nomura, *Scientific reports* **2018**, 8, 1.
[44] C. Dames, G. Chen, CRC press Boca Raton, 2006.
[45] G. Chen, *International journal of thermal sciences* **2000**, 39, 471.
[46] C. S. Gorham, J. T. Gaskins, G. N. Parsons, M. D. Losego, P. E. Hopkins, *Applied Physics Letters* **2014**, 104, 253107.
[47] X. Zhang, H. Xie, M. Fujii, H. Ago, K. Takahashi, T. Ikuta, H. Abe, T. Shimizu, *Applied Physics Letters* **2005**, 86, 171912.

요약(국문초록)

무어의 법칙에 따르면, CPU의 단위 면적당 트랜지스터의 개수는 매 2년마다 두배씩 증가해왔다. 이에 따라, 트랜지스터의 소스와 드레인 사이의 거리는 오늘날 7 nm에 이르게 되었다. 이렇게 길이들이 나노스케일로 줄어들게 되면, 물질의 열 전도 특성 역시 감소하는 경향을 보이는데, 이로 인해 나노스케일에서의 열 관리는 더욱 복잡해지게 된다. 그러므로 CPU의 수명을 길게, 성능을 좋게 만드는 것의 핵심은 실리콘 나노구조체에서의 열 전달에 대한 근원적인 이해라고 할 수 있다.

나노구조에서 열전도도의 감소는 사이즈 효과(size effect)라고도 불리며, 박막이나 나노와이어 같은 부피가 균질한 구조체에서 활발하게 연구되어왔다. 반면에, 온도 기울기 방향으로의 단면적이 일정하지 않은 불균질한 구조에서는 열전도도 감소 메커니즘은 훨씬 복잡해지고, 모델링에 의한 예측값과 실험값에 차이를 보이게 된다.

본 연구에서는, 사다리 모양의 나노래더(nanoladder), 한 쌍의 올곧은 빔과 둘을 이어주는 다수의 다리로 이루어진 구조에서의 포논 전달을 체계적으로 연구하였다. 열전도도의 측정은 두 개의 떠있는 판에 전기적으로 줄 열을 가하는 two-islands 방법을 사용했다. 열전도도의 모델링은 Callaway-Holland 모델링을 기반으로 하였으며, 시뮬레이션을 통한 평균자유행로 계산도 동반되었다. 올곧은 빔과 다리 부분의 단면적의 비를 ~5.3에서 ~1사이의 값으로 변화시키면서, 우리는 열전도도 특성에서 특이한 교차점을 확인하였다. 포논의 산란거리(scattering distance)에 대한 시뮬레이션과 통계적 분석을 이용해, 올곧은 빔을 통해 전달되는 포논들의 전달 특성이 Lévy walk를 따르며, 사다리의 다리 부분으로 이동하는 포논들은 Brownian motion 전달 특성을 따름을 확인하였다.

이러한 발견은, 체계적으로 설계된 비균질한 구조의 특정 부피들에 의해 포논들이 선택적으로 걸러지고, 그에따라 나노스케일에서 열을 비확산적(non diffusive)으로 다룰 수 있음을 시사한다.

주요어 : Nanoladder, Thermal conductivity, Phonon, Lévy walk, Mean free path, Shape parameter, Free path distribution

학 번 : 2019-26383